Molecular Therapy
Original Article

Circular RNA Cdyl promotes abdominal aortic aneurysm formation by inducing M1 macrophage polarization and M1-type inflammation

Haoyu Song,[1,4,7] Yang Yang,[1,2,3,7] Yili Sun,[1,2,3] Guoquan Wei,[1,2,3] Hao Zheng,[1,2,3] Yijin Chen,[1,2,3] Donghua Cai,[1,2,3] Chuling Li,[1,2,3] Yusheng Ma,[1,2,3] Zhongqiu Lin,[1,2,3] Xiaoran Shi,[1,2,3] Wangjun Liao,[6] Yulin Liao,[1,2,3] Lintao Zhong,[1,5] and Jianping Bin[1,2,3]

[1]Department of Cardiology, State Key Laboratory of Organ Failure Research, Nanfang Hospital, Southern Medical University, 1838 Guangzhou Avenue North, Guangzhou 510515, China; [2]Guangzhou Regenerative Medicine and Health Guangdong Laboratory, Guangzhou 510005, China; [3]Guangdong Provincial Key Laboratory of Shock and Microcirculation, Guangzhou 510515, China; [4]Wards of Cadres, Zhuhai People's Hospital (Zhuhai Hospital Affiliated with Jinan University), Zhuhai 519000, China; [5]Department of Cardiology, Zhuhai People's Hospital (Zhuhai Hospital Affiliated with Jinan University), Zhuhai 519000, China; [6]Department of Oncology, Nanfang Hospital, Southern Medical University, Guangzhou 510515, China

Macrophage polarization plays a crucial role in regulating abdominal aortic aneurysm (AAA) formation. Circular RNAs (circRNAs) are important regulators of macrophage polarization during the development of cardiovascular diseases. However, the roles of circRNAs in regulating AAA formation through modulation of macrophage polarization remain unknown. In the present study, we compared circRNA microarray data under two distinct polarizing conditions (M1 and M2 macrophages) and identified an M1-enriched circRNA, circCdyl. Loss- and gain-of-function assay results demonstrated that circCdyl overexpression accelerated angiotensin II (Ang II)- and calcium chloride ($CaCl_2$)-induced AAA formation by promoting M1 polarization and M1-type inflammation, while circCdyl deficiency showed the opposite effects. RNA pulldown, mass spectrometry analysis, and RNA immunoprecipitation (RIP) assays were conducted to elucidate the underlying mechanisms by which circCdyl regulates AAA formation and showed that circCdyl promotes vascular inflammation and M1 polarization by inhibiting interferon regulatory factor 4 (IRF4) entry into the nucleus, significantly inducing AAA formation. In addition, circCdyl was shown to act as a let-7c sponge, promoting C/EBP-δ expression in macrophages to induce M1 polarization. Our results indicate an important role for circCdyl-mediated macrophage polarization in AAA formation and provide a potent therapeutic target for AAA treatment.

INTRODUCTION

Abdominal aortic aneurysm (AAA) is a chronic inflammatory and degenerative disease characterized by inflammation, extracellular matrix (ECM) degradation, and the impairment of vascular smooth muscle cell (VSMC) homeostasis.[1,2] Macrophages, categorized into two subsets known as classically activated macrophages (M1-like) and alternatively activated macrophages (M2-like), play a crucial role in the resolution of the initial inflammatory phase, which dominates the key pathogenesis of AAA and includes matrix degeneration and induction of VSMC apoptosis. Generally, M1 cells exert a proinflammatory effect and induce matrix degeneration, while M2 cells facilitate the resolution of inflammation and alleviate tissue remodeling.[3–7] Macrophage polarization (also known as macrophage activation) has been shown to participate in pathological conditions of the inflammatory system, including the development of kidney disease, chronic pulmonary granulomatous disease, osteoarthritis, and inflammatory bowel disease.[8–12] More importantly, previous studies have identified a phenotypic switch from M2 to M1 and an increase in total macrophage accumulation with a higher M1/M2 ratio, both of which resulted in doubled or tripled aortic diameters and substantially induced AAA formation by enhancing vascular inflammation.[13,14] Emerging evidence has indicated that the regulation of differently polarized macrophages *in situ* may be a potential approach for modulating inflammation and AAA formation.[14] In addition, certain protein-coding genes and microRNAs (miRNAs), such as tumor necrosis factor (TNF)-α, SIRT1, and miR-144-5p, have been shown to regulate AAA formation by mediating macrophage polarization.[15–17] However, the roles and mechanisms by which circRNAs regulate AAA formation through the modulation of macrophage polarization remain unknown.

Noncoding RNAs (ncRNAs), including miRNAs, long noncoding RNAs (lncRNAs), and circular RNAs (circRNAs), have been functionally implicated in mediating macrophage activation during the

Received 11 January 2021; accepted 14 September 2021;
https://doi.org/10.1016/j.ymthe.2021.09.017.

[7]These authors contributed equally

Correspondence: Jianping Bin, MD, PhD, Department of Cardiology, State Key Laboratory of Organ Failure Research, Nanfang Hospital, Southern Medical University, 1838 Guangzhou Avenue North, Guangzhou, 510515, China.
E-mail: jianpingbin@126.com
Correspondence: Lintao Zhong, MD, PhD, Department of Cardiology, Zhuhai People's Hospital (Zhuhai Hospital Affiliated with Jinan University), Zhuhai 519000, China.
E-mail: zhonglintao1991@hotmail.com

development of cardiovascular diseases, such as myocardial ischemia, atherosclerosis, and viral myocarditis.[18–20] CircRNAs are a class of ncRNAs that are synthesized by head-to-tail splicing of linear RNA molecules, which maintains their resistance to ribonuclease (RNase).[21,22] The structural stability, high conservation, tissue specificity, and miRNA/protein-binding capacity of circRNAs make these molecules ideal therapeutic target candidates to regulate disease development.[23,24] Moreover, circRNAs have been shown to control the regulation of vascular remodeling, VSMC apoptosis, cell proliferation, and the inflammatory response.[25–27] CircRNAs also play important roles in regulating inflammation during atherosclerosis, alcoholic liver disease, and adipose inflammation.[28–30] Recently, a microarray analysis comparing the circRNA expression profiles of bone marrow-derived macrophages (BMDMs) under two distinct polarizing conditions (M1 and M2) indicated that circRNA Cdyl (circCdyl) expression changed 7-fold in M1 compared to M2 and that this circRNA is homologous between humans and mice.[31] In addition, the sequence of circCdyl has been shown to be complementary to the seed sequence of let-7c, which is expressed at low levels in AAA tissues and plays a vital role in facilitating M2 polarization, indicating that circCdyl may function as a let-7c sponge to further regulate downstream gene expression during AAA formation.[32,33] Therefore, we postulated that circCdyl is likely to regulate AAA formation by modulating macrophage polarization and M1-type inflammation.

To clarify the underlying mechanism by which circCdyl promotes AAA formation, we conducted RNA pulldown assays of circCdyl and observed that interferon (IFN) regulatory factor 4 (IRF4) was the most abundant among the RNA-binding proteins identified by mass spectrometry analysis. IRF4 has been shown to function as a transcription factor in the nucleus and promote M2 polarization.[34,35] In the present study, we further demonstrated that circCdyl upregulation promoted M1 polarization and stimulated M1-type inflammation by preventing IRF4 from entering the cell nucleus and acting as a sponge for let-7c to promote C/EBP-δ expression in macrophages, significantly aggravating angiotensin II (Ang II)- and calcium chloride ($CaCl_2$)-induced AAA development.

RESULTS

circCdyl expression is associated with AAA formation

A previous study identified circRNAs that are differentially expressed between two distinct polarized patterns of macrophage activation (M1 and M2).[31] Using these microarray data, we selected the top five upregulated and downregulated circRNAs in M1 cells and searched for circRNAs that are conserved between humans and mice to facilitate their translation to clinical use in the future. Considering that overly short or long circRNA sequences are unfavorable for constructing specific primers or effective small interfering RNAs (siRNAs) and overexpression plasmids, we excluded circRNAs less than 400 bp or more than 5,000 bp. Based on the above criteria, we identified three circRNAs (Cdyl, Fut8, and Rnf2) (Figure S1A).

To determine whether these circRNAs are involved in AAA formation, we established Ang II-induced mouse AAA and saline-induced normal aorta (NA) (Figure S1B). The quantitative PCR (qPCR) results showed that the expression of MMP9, MCP1, interleukin (IL)-6, and TNF-α was upregulated in mouse AAA (Figure S1C). Of the three circRNAs, circCdyl was most enriched in AAA tissues (Figure 1A). To determine the expression of circCdyl during the development of AAA, we assessed circCdyl mRNA expression at 3, 7, and 14 days after Ang II infusion. We observed elevated circCdyl mRNA on the third day and throughout the disease process (Figure S1D). Based on the above evidence, circCdyl was chosen for further detailed analysis and functional characterization.

Divergent primers amplified circCdyl from cDNA but not from genomic DNA, indicating that this RNA species is circular in form (Figure 1B). The circCdyl nucleotide sequence was strongly conserved, with >95% homology among humans, rats, and mice (Figure 1C). qPCR results demonstrated that circCdyl had greater stability than the linear transcript when treated with RNase or actinomycin D (Figures 1D and 1E). In addition, no difference in linear Cdyl was observed between macrophages stimulated with lipopolysaccharide (LPS) and IFN-γ and control macrophages (Figures S2C–S2E). Similarly, linear Cdyl in mouse AAA tissues did not differ from that observed in NA tissues. In addition, we studied the role of linear Cdyl in macrophages and observed that linear Cdyl overexpression had no effect on the expression of inducible nitric oxide synthase (iNOS), Arg1, and MMP9 in macrophages stimulated with LPS and IFN-γ. The different trends for circCdyl and linear Cdyl transcript expression suggest an important function of circCdyl. To determine the distribution of circCdyl, mouse vascular, liver, lung, brain, heart, and muscle tissues were collected, and the qPCR results showed that circCdyl was expressed in these tissues and was enriched in the vascular tissue (Figure 1F). Moreover, we detected circCdyl expression in macrophages, VSMCs, and endothelial cells, which are cell types that mediate inflammation during AAA. We observed that circCdyl was highly expressed in mouse macrophage RAW264.7 cells and primary macrophages compared to other cell types (Figure 1G). We then separated cytoplasmic RNA and nuclear RNA, and circCdyl was observed to be primarily located in the cytoplasm of macrophages (Figure 1H). Moreover, *in situ* hybridization (ISH) showed that circCdyl was highly accumulated in the vascular wall of AAA (Figure 1I). Finally, to further investigate the expression of circCdyl in human AAA, we collected human AAA tissues and their control adjacent aortic sections without aneurysms from patients undergoing open surgery. Immunohistochemical (IHC) results revealed the decrease of smooth muscle 22α (SM22α, a marker of VSMC) expression in human AAA, which confirmed characteristics of AAA (Figure S1E). We observed that circCdyl mRNA levels were also upregulated in human AAA tissues (Figure 1J).

These results indicate that circCdyl may be involved in AAA formation.

circCdyl knockdown promotes Ang II-induced AAA formation

To evaluate the effect of circCdyl on AAA, we constructed an adeno-associated virus serotype 2 (AAV2) construct to knock down

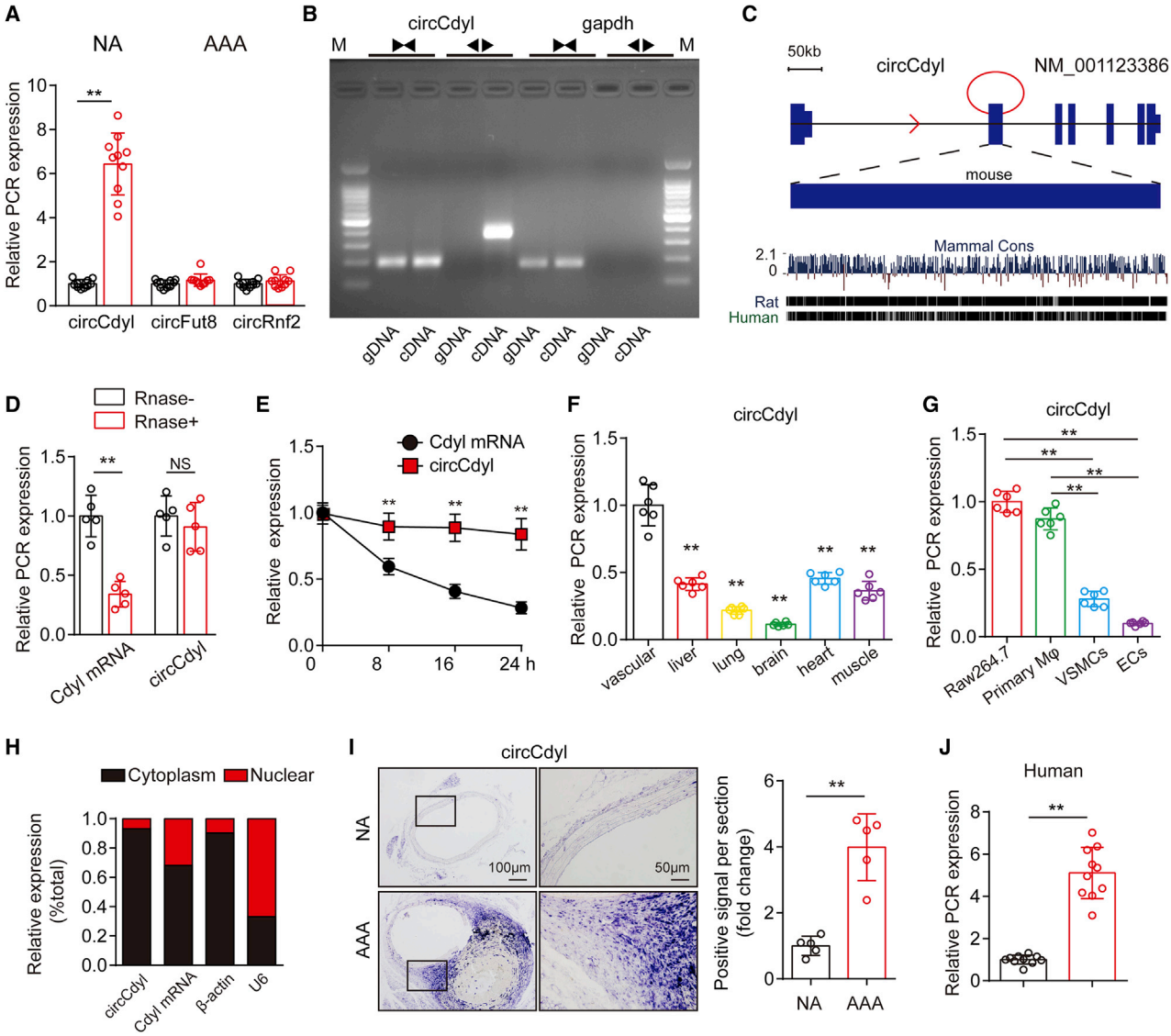

Figure 1. circCdyl is significantly upregulated in AAA

(A) Relative expression of circCdyl, circFut8, and circRnf2 in mouse AAA and NA tissues (qPCR). **p < 0.01 versus the NA group; n = 10 per group. (B) Divergent primers amplify circCdyl from cDNA but not genomic DNA (gDNA); the divergent and convergent primers are indicated by the direction of the arrow. (C) Mouse genomic loci of the circCdyl in Cdyl genes. The expression of circCdyl was validated by reverse transcriptase polymerase chain reaction (RT-PCR) followed by Sanger sequencing. Its conserved analogs in humans, rats, and mice, as well as the per base conservation score, are also depicted. (D) Abundances of circCdyl and Cdyl mRNA in RAW264.7 cells treated with RNase R ($RNase^+$) or untreated ($RNase^-$). **p < 0.01 versus $RNase^-$; NS, not significant versus $RNase^-$; n = 5 per group. (E) Abundances of circCdyl and Cdyl mRNA in RAW264.7 cells treated with actinomycin D at the indicated time points (qPCR). **p < 0.01 versus Cdyl mRNA; n = 6 per group. (F) Relative expression of circCdyl in multiple mouse tissues (qPCR). **p < 0.01 versus vascular tissue; n = 6 per group. (G) Relative expression of circCdyl in several vascular cell types (qPCR). **p < 0.01 versus; n = 6 per group. (H) Abundance of circCdyl and Cdyl mRNA in either the cytoplasm or nucleus of RAW264.7 cells (qPCR). (I) *In situ* hybridization and densitometric analysis of aortic circCdyl in Ang II-treated mice (scale bars, 200 and 50 mm). **p < 0.01 versus NA; n = 5 per group. (J) Relative expression of circCdyl in human AAA and NA tissues (qPCR). **p < 0.01 versus NA; n = 10 per group.

circCdyl (Sh-circCdyl). Male $ApoE^{-/-}$ mice were randomly allocated to two groups and transfected with Sh-circCdyl or negative control virus (Scr-RNA). To determine the intervention effect, aortas were collected from the mice in the two groups on the 30th day. The qPCR results showed that circCdyl mRNA expression was inhibited in the Sh-circCdyl group compared to the Scr-RNA group (Figure S3A), suggesting that the transfection was successful. According to the results of previous studies, AAV2 viruses typically displayed relatively higher transfection efficiency in macrophages. *In vivo*, they usually take effect 15 days after

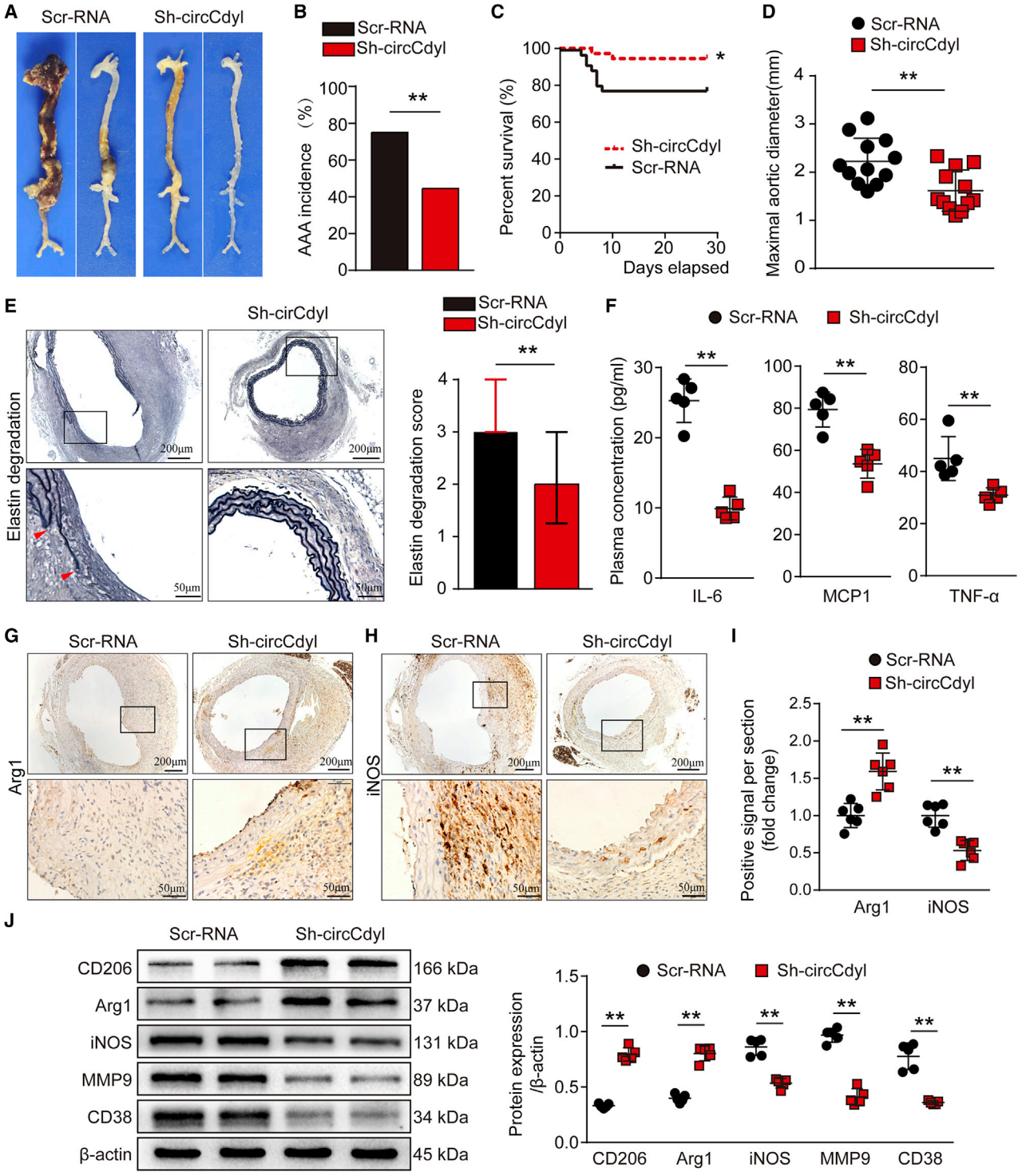

Figure 2. Knockdown of circCdyl attenuates Ang II-induced AAA formation and decreases the levels of inflammatory molecules associated with M1 macrophages

(A) Images showing the characteristics of aortas from Ang II-infused ApoE$^{-/-}$ mice transfected with circCdyl-knockdown AAV (Sh-circCdyl) or corresponding control AAV (Scr-RNA). (B) Incidence of AAA in Ang II-infused ApoE$^{-/-}$ mice in the two indicated groups. **p < 0.01; n = 36 per group. (C) Survival curves of Ang II-infused ApoE$^{-/-}$ mice in

(legend continued on next page)

transfection and reach a relative high effect at 1 month, and they can last for more than 2 months.[36,37] Therefore, we generated Ang II-infused AAA models in the two groups of mice on the 30th day after viral transfection. Blood pressure is an important factor contributing to AAA formation.[38,39] Our results showed that Ang II infusion markedly increased the systolic blood pressure of mice in both the Sh-circCdyl and Scr-RNA groups during the experimental period, but there were no significant differences between mice in the two groups (Figure S3B).

After 28 days of Ang II infusion, all mice were sacrificed and the aortas were collected. The incidence of AAA induced by Ang II infusion was 44.4% and 75% in the Sh-circCdyl group mice and the Scr-RNA group mice, respectively (Figures 2A and 2B). During the Ang II infusion period, vascular ultrasound imaging showed milder dilation in the abdominal aorta of mice in the Sh-circCdyl group compared to those in the Scr-RNA group on the 14th and 28th days (Figure S3C). circCdyl knockdown markedly decreased the mortality caused by aortic rupture of Ang II-induced AAA (Figure 2C). Mice in the Sh-circCdyl group also exhibited lower lumen diameters both on the 14th and the 28th days (Figure S3D). The maximal outer diameter of the abdominal aorta from mice in the Sh-circCdyl group was significantly smaller than that of mice in the Scr-RNA group (Figure 2D). Histological analysis showed that mice in the Sh-circCdyl group exhibited a milder elastic degradation (Figure 2E). In addition, blood samples were collected from aortas to separate the plasma for the detection of inflammatory cytokines. The results showed that the plasma concentrations of IL-6, MCP1, and TNF-α in mice in the Sh-circCdyl group were all significantly decreased (Figure 2F). We next investigated whether circCdyl could influence macrophage polarization *in vivo*. The immunochemical staining results showed that the expression of Arg1, a marker of M2 macrophages, was upregulated in aortic walls in Sh-circCdyl group mice, while the levels of the M1 markers iNOS and MMP9 and the inflammatory factors MCP1 and IL-6 were decreased (Figures 3G–3I; Figures S4A–S4C). IHC staining of CD68 also revealed less macrophage infiltration in the Sh-circCdyl group than in the Scr-RNA group (Figure S4D). The western blot results revealed upregulation of the M2-related markers CD206 and Arg1 and a reduction of the M1-related markers iNOS, MMP9, and CD38 (Figure 2J). Flow cytometry analysis confirmed the increase of $CD206^{+}CD86^{-}$ M2 macrophages and decrease of $CD86^{+}CD206^{-}$ M1 macrophages after knockdown of circCdyl (Figure S5).

Overall, these results showed that knockdown of circCdyl attenuated Ang II-induced AAA formation.

circCdyl overexpression promotes Ang II-induced AAA formation

We next examined the effects of circCdyl overexpression on AAA. C57BL/6J mice were randomly divided into two groups and transfected with a circCdyl overexpression AAV2 (AAV-circCdyl) and a corresponding sham control virus (AAV-GFP). The qPCR results showed that circCdyl mRNA expression was increased in the aortas of mice in the AAV-circCdyl group (Figure S6A), while no difference in the systolic blood pressure of mice was observed between the two groups (Figure S6B).

The results showed that Ang II stimulation could significantly induced AAA in C57BL/6J mice transfected with AAV-circCdyl (Figure 3A). Ultrasound imaging showed progressively greater dilation of mice in the AAV-circCdyl group compared to that observed in the AAV-GFP group (Figures S6C and S6D). Overexpression of circCdyl significantly increased the incidence of Ang II-induced AAA (Figure 3B). Both the mortality and maximal abdominal aortic diameter were markedly increased in AAV-circCdyl group mice (Figures 3C and 3D). In addition, we assessed the elastin of vessels by elastic van Gieson (EVG) staining. The results showed that overexpression of circCdyl further exacerbated Ang II-induced elastin degradation (Figure 3E). Concomitantly, plasma IL-6, MCP1, and TNF-α concentrations were increased in the AAV-circCdyl group mice (Figure 3F). IHC staining showed that Ang II increased the expression of iNOS and MMP9, markers of M1 macrophages, in mice in the AAV-circCdyl group (Figures 3G–3I). The expression of MCP1 and IL-6 was also increased and macrophage infiltration (CD68) was more obvious in the AAV-circCdyl group (Figures S7A–S7C). The western blot results also showed that circCdyl overexpression increased iNOS, MMP9, and CD38 levels in the mouse aortas (Figure 3J). Consistently, flow cytometry analysis revealed that circCdyl overexpression increased M1 macrophages while it decreased M2 macrophages (Figure S8).

These results suggest that overexpression of circCdyl promotes mouse Ang II-induced AAA formation and increases inflammatory conditions associated with M1 macrophages.

circCdyl overexpression promotes $CaCl_2$-induced AAA formation

To further validate the role of circCdyl in AAA, we examined the effects of circCdyl overexpression in another mouse AAA model; that is, $CaCl_2$-induced AAA model mice were evaluated.

Consistent with the abovementioned results, overexpression of circCdyl increased the maximal abdominal aortic diameter in

the two indicated groups. *$p < 0.05$; n = 36 per group. (D) Maximal abdominal aortic outer diameters in Ang II-infused $ApoE^{-/-}$ mice in the two indicated groups. **$p < 0.01$; n = 12 per group. (E) EVG staining images and elastin degradation scores in the two indicated groups (scale bars, 200 and 50 μm). **$p < 0.01$; n = 12 per group. (F) Plasma concentrations of IL-6, MCP1, and TNF-α from aortas of Ang II-infused $ApoE^{-/-}$ mice in the two indicated groups. **$p < 0.01$; n = 5 per group. (G–I) Immunohistochemical staining of Arg1 (G) and iNOS (H) and corresponding densitometric analysis (I) in the aortas of Ang II-infused $ApoE^{-/-}$ mice in the two indicated groups (scale bars, 200 and 50 μm). **$p < 0.05$; n = 6 per group. (J) CD206, Arg1, iNOS, MMP9, and CD38 levels in the aortas of Ang II-infused $ApoE^{-/-}$ mice in the two indicated groups (western blot) (β-actin as the internal reference). **$p < 0.01$; n = 5 per group.

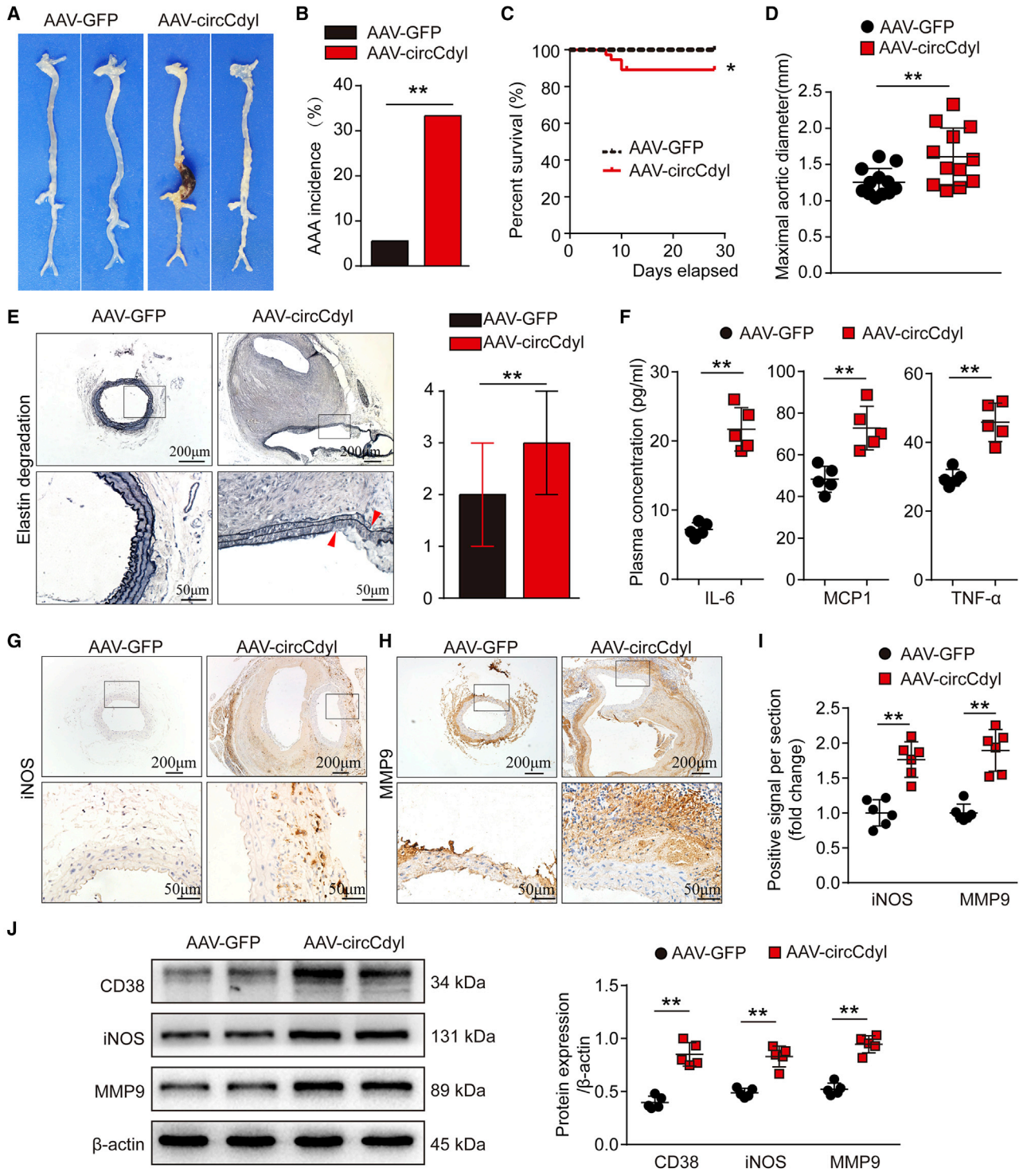

Figure 3. Overexpression of circCdyl promotes Ang II-induced AAA formation and increases the levels of inflammatory molecules associated with M1 macrophages

(A) Images showing the characteristics of aortas from Ang II-infused C57BL/6J mice transfected with circCdyl-overexpressing AAV (AAV-circCdyl) or corresponding control AAV (AAV-GFP). (B) Incidence of AAA in Ang II-infused C57BL/6J mice in the two indicated groups. **$p < 0.01$; n = 36 per group. (C) Survival curves of Ang II-infused C57BL/6J mice in the two indicated groups. *$p < 0.05$; n = 36 per group. (D) Maximal abdominal aortic outer diameters from Ang II-infused C57BL/6J mice in the two indicated

(legend continued on next page)

$CaCl_2$-treated mice (Figures S9A and S9B). EVG staining showed that the elastic lamellae were disrupted and degraded to a greater extent in the AAV-circCdyl group (Figures S9C and S9D). IHC results revealed that overexpression of circCdyl significantly enhanced the expression of iNOS, MMP9, MCP1, and IL-6, as well as macrophage infiltration, indicating the promoting effect of circCdyl on M1 macrophage polarization (Figures S9E–S9G S10A–S10C). Furthermore, we collected blood samples from aortas and detected the levels of inflammatory factors in plasma. As expected, overexpression of circCdyl elevated the serum levels of TNF-α, IL-1β, and IL-6 compared to those in the AAV-GFP group (Figure S9H). In addition, western blot showed that CD38, iNOS, and MMP9 protein levels were increased in the AAV-circCdyl group (Figures S9I and S9J).

Taken together, these results further indicated that circCdyl overexpression promoted AAA formation in $CaCl_2$-induced models.

circCdyl promotes M1 polarization by inhibiting the entry of IRF4 into the nucleus

To better elucidate the function of circCdyl in macrophages, we performed RNA pulldown assays of circCdyl using biotinylated probes targeting the circCdyl backspliced sequence (Figure 4A), and the precipitates were subjected to mass spectrometry analysis. Several RNA-binding proteins were identified by mass spectrometry analysis (Table S5), the most abundant of which was IRF4, which has been reported to promote the macrophage M2 program.[34,35] The interaction between circCdyl and IRF4 was confirmed through RNA pulldown followed by western blotting and RNA immunoprecipitation (RIP) (Figures 4A and 4B). Next, we investigated the molecular consequences of the interaction between circCdyl and IRF4. Mouse peritoneal macrophages were collected from C57BL/6J mice and then transfected with siRNA against circCdyl (si-circCdyl), scramble siRNA (si-scramble), a circCdyl overexpression plasmid (oe-circCdyl), or the corresponding negative control plasmid (oe-vector). The qPCR and western blot results showed that the IRF4 mRNA and protein levels were not altered when circCdyl was inhibited or overexpressed (Figures 4C–4E), suggesting that the effect of circCdyl on IRF4 may occur through alternate means.

As IRF4 has been reported to be a transcription factor that functions in the nucleus; therefore, we subsequently explored the effect of circCdyl on the entry of IRF4 into the nucleus.[40] Mouse peritoneal macrophages were transfected with oe-circCdyl or oe-vector and then stimulated with 20 ng/mL IL-4 for 24 h to induce M2 phenotype macrophages. Cytoplasmic and nuclear proteins were extracted separately to determine the level of IRF4 in the cytoplasm and nucleus. The western blot results showed that IRF4 protein levels were elevated in the cytoplasm but decreased in the nucleus upon IRF4 overexpression (Figures 4F and 4G). In addition, mouse peritoneal macrophages were transfected with si-circCdyl or si-scramble and stimulated with IL-4. The results showed that IRF4 protein levels were decreased in the cytoplasm and increased in the nucleus (Figures 4H and 4I). The above results suggest that circCdyl inhibits the entry of IRF4 into the nucleus.

Subsequently, we assessed whether circCdyl impacts macrophage polarization through its interaction with IRF4. To this end, RAW264.7 macrophages were treated with IL-4 to induce M2 polarization and then transfected with oe-vector, oe-circCdyl, or oe-circCdyl together with an IRF4 overexpression plasmid (oe-IRF4). Flow cytometry analysis showed that circCdyl overexpression decreased the proportion of M2 macrophages. However, IRF4 overexpression reversed this inhibitory effect of circCdyl overexpression on M2 polarization (Figures 5A and 5B). Then, we analyzed the effects of circCdyl overexpression on the M1 polarization of macrophages. To this end, we stimulated RAW264.7 macrophages with 100 ng/mL LPS and 50 ng/mL IFN-γ for 24 h to induce M1 polarization. The overexpression of circCdyl increased the M1 proportion in LPS+IFN-γ-treated macrophages, whereas IRF4 reversed this effect (Figures 5C and 5D). We further investigated the effect of circCdyl knockdown on macrophage polarization and observed that, conversely, circCdyl knockdown (si-circCdyl) promoted M2 polarization induced by IL-4 and inhibited M1 polarization induced by LPS and IFN-γ. Furthermore, IRF4 knockdown (si-IRF4) abolished the effects of circCdyl knockdown on macrophage polarization (Figures 6A–6D). The results were consistent with the western blot findings for the M1 marker proteins CD38, iNOS, and MMP9 and the M2 marker proteins CD206 and Arg1 in mouse peritoneal macrophages and human THP-1 cells treated with IL-4 or LPS+IFN-γ (Figures 7A–7D; Figures S11A–S11D).

As ECs and VSMCs are important sources of aortic inflammation during AAA formation, we assessed the effect of circCdyl in the two cell types. We observed that circCdyl overexpression had no effect on the expression of inflammation factors in ECs (iNOS, MCP1, and ICAM-1) (Figures S12A–S12C) and VSMCs (IL-6, MCP1, and MMP2) (Figures S12D–S12F). These results suggest that circCdyl primarily affects the inflammation status of macrophages.

Overall, we demonstrated that circCdyl promotes M1 polarization by binding IRF4 and inhibiting its entry into the nucleus.

circCdyl acts as a sponge for let-7c and promotes C/EBP-δ expression in macrophages

circRNAs often function through a competing endogenous RNA (ceRNA) mechanism. As circCdyl is abundant in the cytoplasm, we

groups. **p < 0.01; n = 12 per group. (E) EVG staining images and elastin degradation score in the two indicated groups (scale bars, 200 and 50 μm). **p < 0.01; n = 12 per group. (F) Plasma concentrations of IL-6, MCP1, and TNF-α in the aortas of Ang II-infused C57BL/6J mice in the two indicated groups. **p < 0.01; n = 5 per group. (G–I) Immunohistochemical staining of iNOS (G) and MMP9 (H) and corresponding densitometric analysis (I) in aortas from Ang II-infused C57BL/6J mice in the two indicated groups (scale bars, 200 and 50 μm). **p < 0.01; n = 6 per group. (J) CD38, iNOS, and MMP9 levels in the aortas of Ang II-infused C57BL/6J mice in the two indicated groups (western blot) (β-actin as the internal reference). **p < 0.01; n = 5 per group.

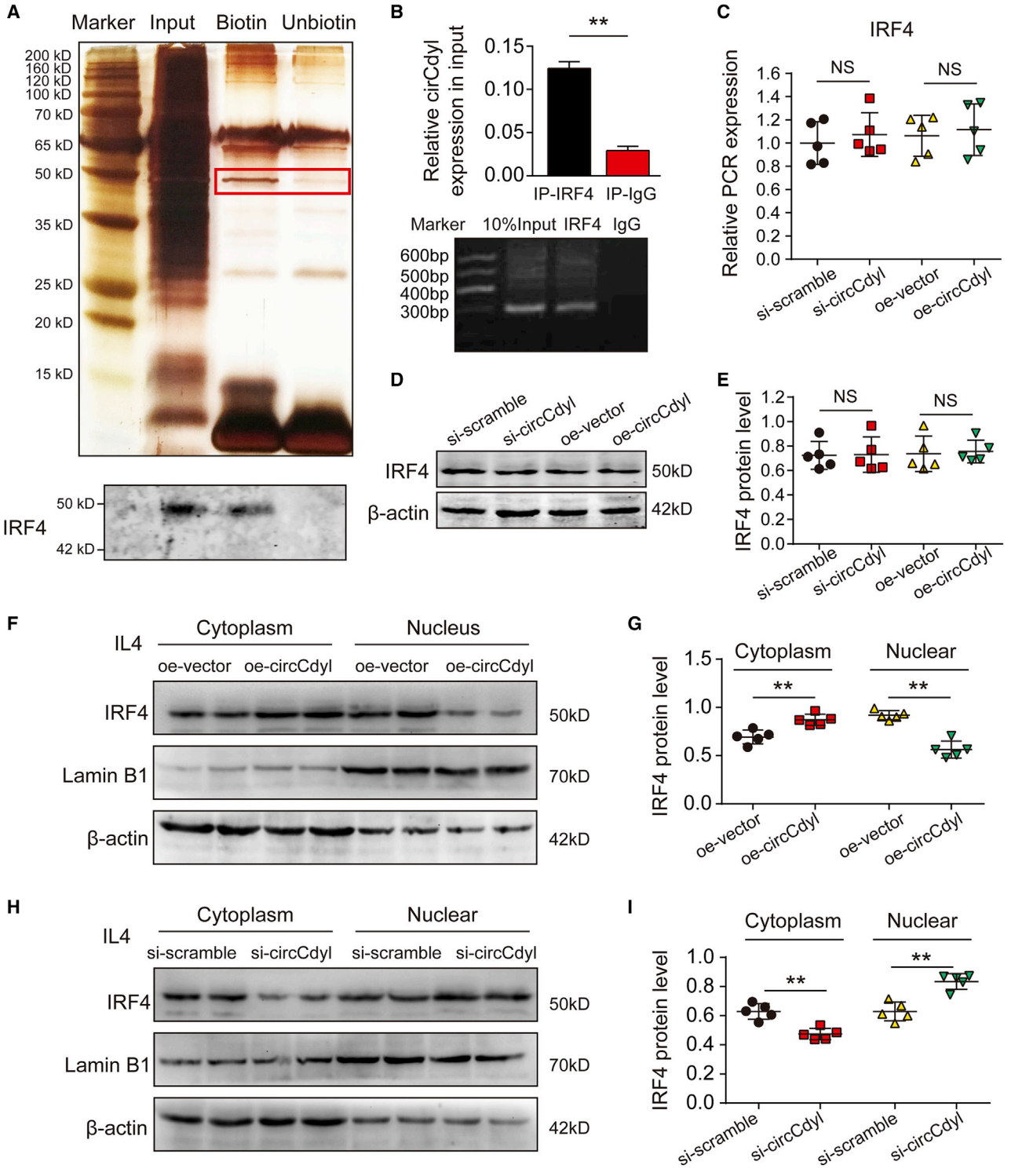

Figure 4. circCdyl binds to IRF4 and inhibits its entry into the nucleus

(A) Silver-stained sodium dodecyl sulfate polyacrylamide gel electrophoresis gel of proteins immunoprecipitated by circCdyl and its antisense circRNA. The red box indicates the region of the gel that was excised and processed for mass spectrometry. IRF4 protein expression was assayed by western blotting. (B) RNA immunoprecipitation (RIP) experiments were performed using an antibody against IRF4 or negative immunoglobulin G (IgG). **$p < 0.01$ versus IgG; n = 3 per group. RIP-derived RNA was measured by

(legend continued on next page)

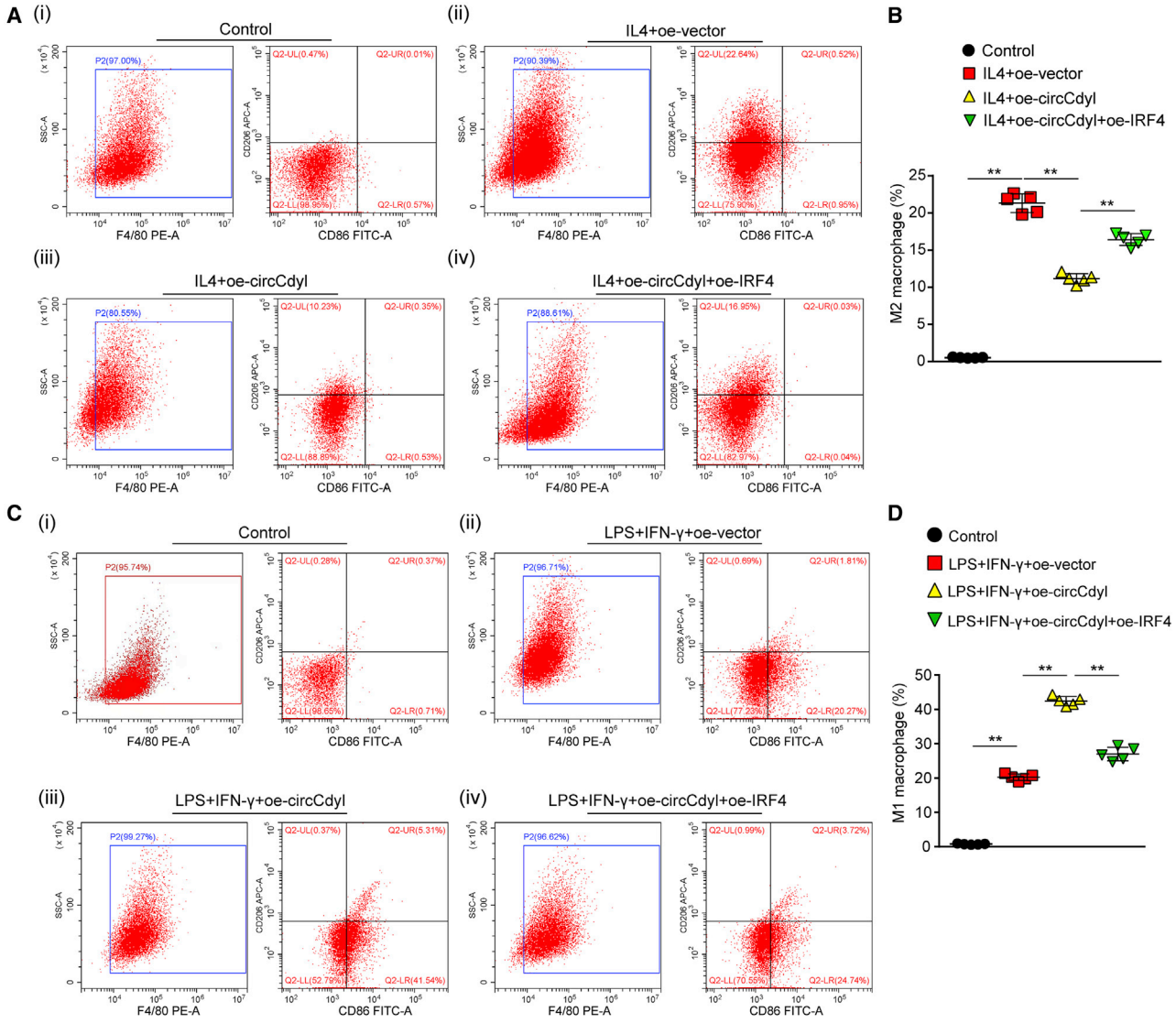

Figure 5. Overexpression of IRF4 inhibits circCdyl induced M1 polarization

(A and C) Flow cytometry plots and quantitative analysis of macrophage differentiation in Raw264.7 cells treated with or without IL-4 (20 ng/mL) and transfected with oe-vector, oe-circCdyl, or oe-circCdyl together with oe-IRF4. **p < 0.01; n = 5 per group. (B and D) Flow cytometry plots and quantitative analysis of macrophage differentiation in Raw264.7 cells treated with or without LPS (100 ng/mL) and IFN-γ (50 ng/mL) and transfected with oe-vector, oe-circCdyl, or oe-circCdyl together with oe-IRF4. **p < 0.01; n = 5 per group.

next hypothesized that circCdyl also functions in this manner. Therefore, using the RNA22 v2 miRNA target detection bioinformatics tool, we observed that the seed sequence of let-7c was complementary to the sequence of circCdyl (Figure S13A). Importantly, let-7c was reported by previous studies to be expressed at low levels in AAA tissues and to play a crucial role in promoting M2 macrophage polarization by targeting C/EBP-δ.[32,33] Based on these results, we next generated luciferase constructs with wild-type circCdyl (circCdyl-WT) and a

qPCR analysis, and IRF4 was expressed as a percentage of the input. (C) Total IRF4 mRNA expression in peritoneal macrophages in which circCdyl was inhibited or overexpressed (detected by qPCR). NS, not significant; n = 5 per group. (D and E) Total IRF4 protein levels in peritoneal macrophages in which circCdyl was inhibited or overexpressed (detected by western blotting, β-actin as the internal reference). NS, not significant; n = 5 per group. (F and G) Cytoplasmic and nuclear IRF4 protein levels in peritoneal macrophages stimulated with IL-4 and overexpressing circCdyl (detected by western blotting, β-actin as the internal reference). **p < 0.01; n = 5 per group. (H and I) Cytoplasmic and nuclear IRF4 protein levels in peritoneal macrophages stimulated with IL-4 and silenced for circCdyl (detected by western blotting, β-actin as the internal reference). **p < 0.01; n = 5 per group.

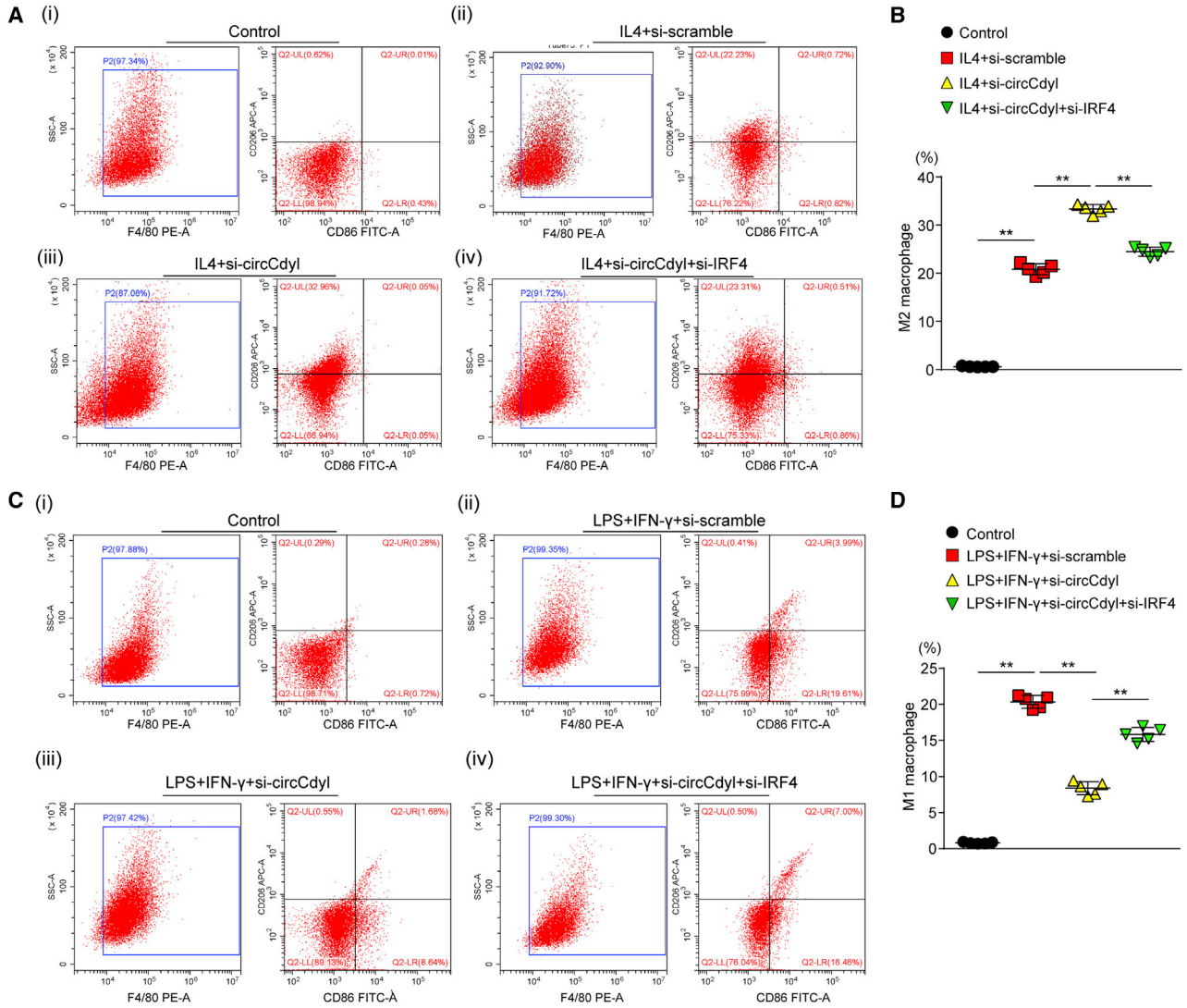

Figure 6. Knockdown of IRF4 circCdyl abolishes circCdyl knockdown induced M2 polarization

(A and C) Flow cytometry plots and quantitative analysis of macrophage differentiation in Raw264.7 cells treated with or without IL-4 (20 ng/mL) and transfected with si-scramble, si-circCdyl, or si-circCdyl together with si-IRF4. **$p < 0.01$; n = 5 per group. (B and D) Flow cytometry plots and quantitative analysis of macrophage differentiation in Raw264.7 cells treated with or without LPS (100 ng/mL) and IFN-γ (50 ng/mL) and transfected with si-scramble, si-circCdyl, or si-circCdyl together with si-IRF4. **$p < 0.01$; n = 5 per group.

mutated form devoid of the let-7c binding site (circCdyl-mut). The results showed that in mouse RAW264.7 cells, let-7c suppressed the luciferase activity of Luc-circCdyl-WT but had a lower effect on Luc-circCdyl-mut (Figure 8A), further indicating that circCdyl directly binds let-7c.

Next, to determine the direct interactions between let-7c and the C/EBP-δ 3′ UTR, we generated luciferase constructs with wild-type C/EBP-δ (C/EBP-δ-WT) and a mutated let-7c binding site construct (C/EBP-δ-mut). Consistent with a previous study showing that let-7c inhibits C/EBP-δ expression, the luciferase reporter assay results showed that in macrophages, let-7c directly targets C/EBP-δ (Figure 8B). The overexpression of circCdyl increased the luciferase activity of C/EBP-δ-WT, which was inhibited by let-7c mimics, while circCdyl overexpression had no impact on the luciferase activity of C/EBP-δ-mut (Figure 8C). The western blot results showed that C/EBP-δ expression was markedly reduced by transfection with let-7c mimics and increased by transfection with let-7c inhibitors in RAW264.7 cells (Figures 8D and 8E). We also observed that C/EBP-δ expression was significantly upregulated after transfection with oe-circCdyl (Figures 8F and 8G), while a let-7c mimic abolished the promoting effect of circCdyl on C/EBP-δ (Figures 8H and HI).

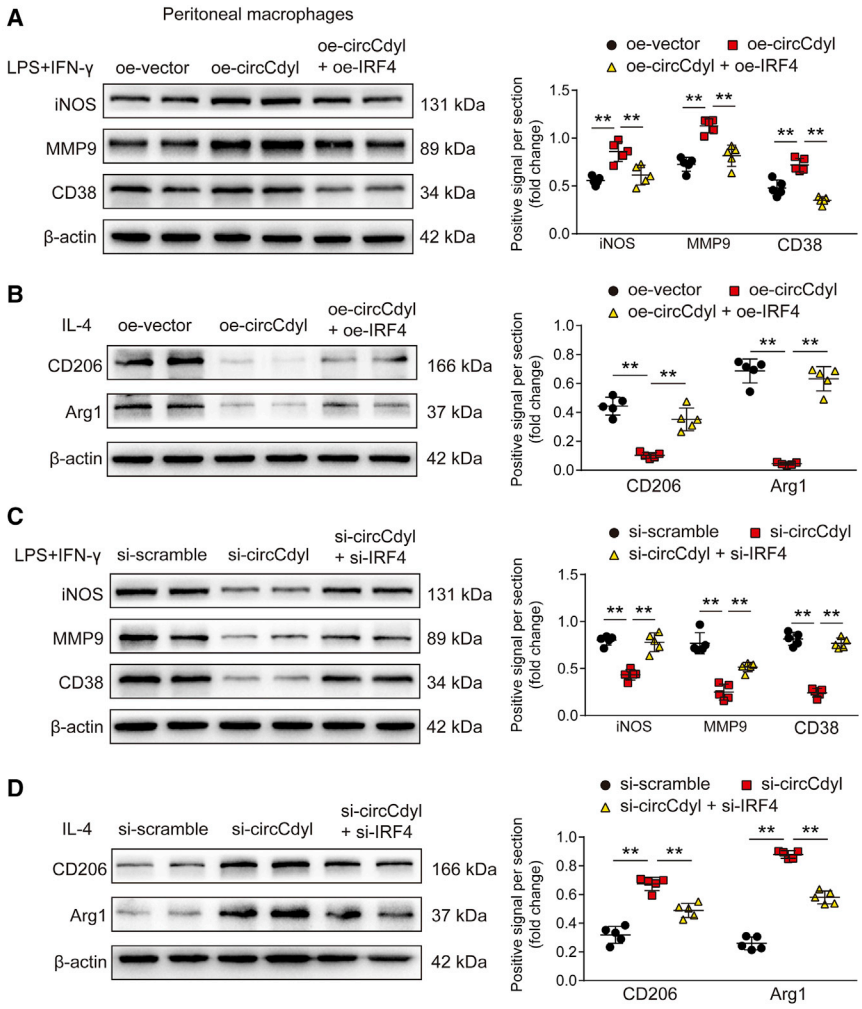

Figure 7. circCdyl induces M1 macrophage polarization through its interaction with IRF4.

(A) iNOS, MMP9, and CD38 protein levels in peritoneal macrophages transfected with oe-vector, oe-circCdyl, or oe-circCdyl + oe-IRF4 and then stimulated with LPS+IFN-γ (24 h). **p < 0.01; n = 5 per group. (B) CD206 and Arg1 protein levels in peritoneal macrophages transfected with oe-vector, oe-circCdyl, or oe-circCdyl + oe-IRF4 and then stimulated with IL-4 (24 h). **p < 0.01; n = 5 per group. (C) iNOS, MMP9, and CD38 protein levels in peritoneal macrophages transfected with si-scramble, si-circCdyl, or si-circCdyl + si-IRF4 and then stimulated with LPS+IFN-γ (24 h). **p < 0.01; n = 5 per group. (D) CD206 and Arg1 protein levels in peritoneal macrophages transfected with si-scramble, si-circCdyl, or si-circCdyl + si-IRF4 and then stimulated with IL-4 (24 h). **p < 0.01; n = 5 per group.

Moreover, we also showed that circCdyl knockdown significantly repressed C/EBP-δ expression, which was reversed by let-7c inhibitors (Figures 8J and 8K). Notably, IRF4 overexpression did not affect the expression of circCdyl or the let-7c-C/EBP-δ pathway (Figures S13B–S13D), demonstrating that another downstream target of circCdyl, IRF4, does not affect the circCdyl/let-7c pathway by feedback regulation of circCdyl or directly interact with let-7c-C/EBP-δ pathway.

Collectively, these findings indicated that circCdyl acts as a sponge for let-7c and increases C/EBP-δ expression in macrophages to promote M1 polarization.

DISCUSSION

In the present study, we identified an M1-enriched circRNA, circCdyl, and demonstrated that circCdyl overexpression induced Ang II- and $CaCl_2$-induced AAA formation by promoting M1 polarization and M1-type inflammation. Mechanistically, upregulated circCdyl promoted M1 polarization by preventing IRF4 from entering the cell nucleus and acting as a let-7c sponge to stimulate C/EBP-δ expression.

First, we provide evidence that circRNAs are involved in macrophage polarization, as M1-enriched circCdyl positively regulated M1 polarization both *in vitro* and *in vivo*. We further demonstrated that downregulated circCdyl inhibited M1 macrophage polarization, which was sufficient to attenuate AAA formation, while linear Cdyl had no effect on macrophage polarization.[15–17] Along with macrophage polarization, circCdyl knockdown notably mitigated the vascular inflammatory response and elastin degradation, which are known to induce AAA formation and even rupture.[13,14] Given that Ang II-induced C57BL/6J mice exhibited much lower AAA incidence and mortality than did $ApoE^{-/-}$ mice, we also assessed these effects in Ang II-induced C57BL/6J mice and observed that circCdyl overexpression significantly promoted aortic enlargement and elastin degradation by stimulating M1 polarization and M1-type inflammation, indicating that circCdyl upregulation was sufficient to aggravate AAA formation.[41,42] Recently, several studies have indicated that mRNAs and miRNAs have important roles in regulating AAA formation by modulating macrophage polarization.[15–17] Our study showed that circCdyl expression was clearly upregulated in human aortic aneurysms compared to normal human aortas. Thus, targeting circCdyl may be a potent therapeutic strategy to inhibit AAA formation.

Previous studies have reported that circRNA usually exerts synergistic effects with its originated gene in the biological process.[25,43,44] For example, both SIRT1 and its circular transcript can regulate vascular inflammation through inhibition of nuclear factor κB (NF-κB). In addition, the siRNA designed for the circRNA often has some intervention effects on the linear mRNA. Therefore, except for the role of circCdyl on macrophage polarization and AAA formation, it is

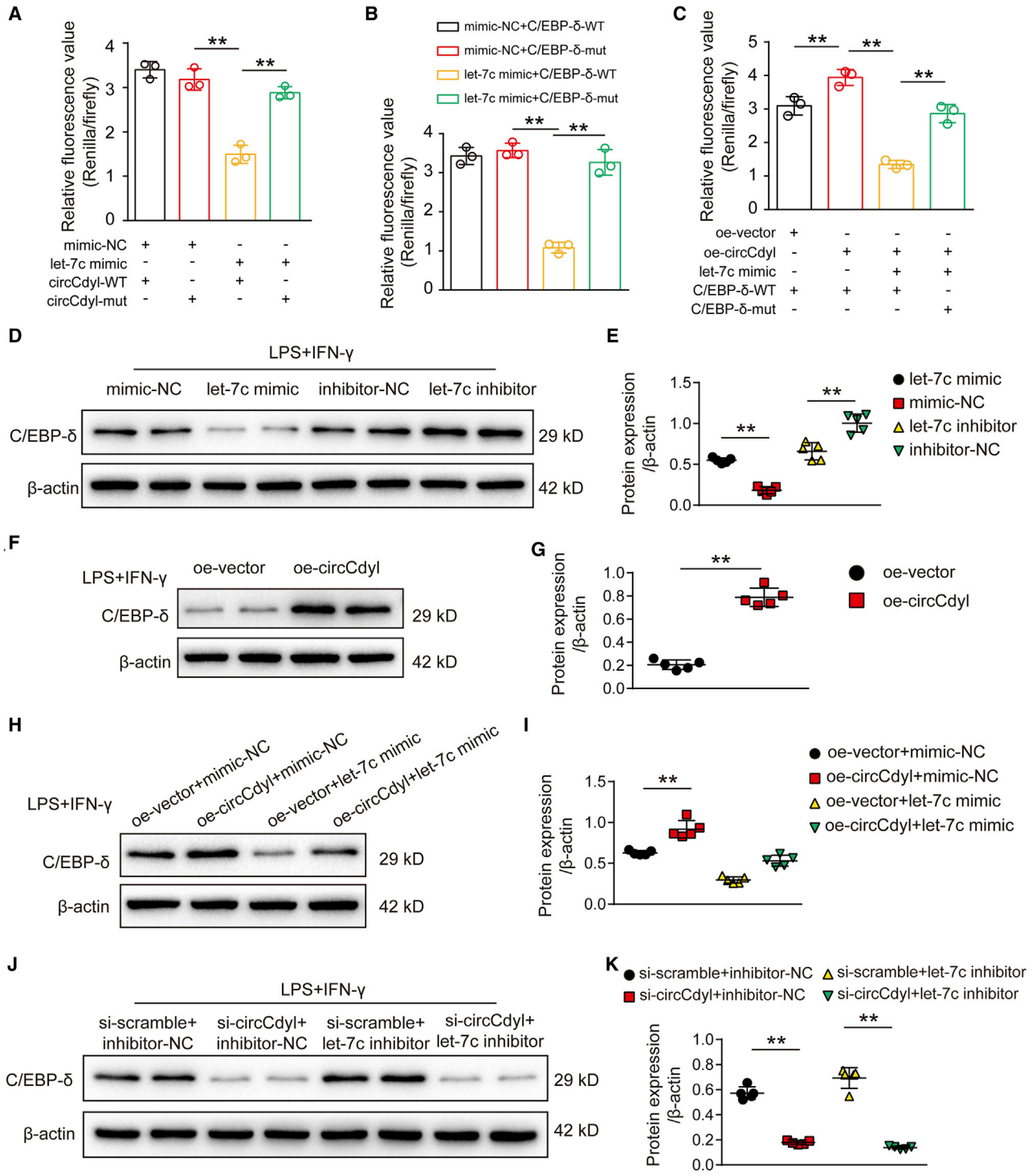

Figure 8. circCdyl acts as a sponge for let-7c and promotes C/EBP-δ expression in macrophages

(A) Results of luciferase reporter assays. RAW264.7 cells were cotransfected with let-7c mimic or mimic-NC and a luciferase reporter containing wild-type circCdyl (circCdyl-WT) or mutant circCdyl (circCdyl-mut). Luciferase activity was analyzed after 24 h. **$p < 0.01$; $n = 3$ per group. (B) Results of luciferase reporter assays. RAW264.7 cells were cotransfected with let-7c mimic or mimic-NC and a luciferase reporter containing wild-type C/EBP-δ (C/EBP-δ-WT) or mutant C/EBP-δ (C/EBP-δ-mut). Luciferase activity was analyzed after 24 h. **$p < 0.01$; $n = 3$ per group. (C) Results of luciferase reporter assays. RAW264.7 cells were cotransfected with or without let-7c mimic, oe-circCdyl or oe-vector, and C/EBP-δ-WT or C/EBP-δ-mut. Luciferase activity was analyzed after 24 h. **$p < 0.01$; $n = 3$ per group. (D and E) C/EBP-δ protein levels in RAW264.7 cells

(legend continued on next page)

crucial to investigate whether linear Cdyl affects the M1/M2 status of macrophages. Our results showed that the level of linear Cdyl did not increase in M1 macrophages or mouse AAA tissues. Also, overexpression of linear Cdyl had no effect on macrophage polarization. The different expression trend and effect for circCdyl and the linear transcript indicate an important role of circCdyl in macrophage polarization. In addition, it is also important to investigate whether the remaining ncRNAs from the same originated gene are differentially expressed. Cdyl transcribes three circularizing transcript variants (transcript variants in the circBase database). In the process of screening the target gene from microarray data, we observed that only the target circCdyl transcript (derived from the backsplicing of exon 2, circBase: mmu_circ_0000451) was differently expressed between M1 and M2 macrophages, while the other two transcripts had no differences in expression.

To better understand the crucial role of circCdyl in AAA formation, we elucidated two mechanisms through which circCdyl fulfills its functions. circRNAs often associate with RNA-binding proteins to exert their biological functions. Using the RNA pulldown, mass spectrometry, and RIP approaches, we demonstrated that circCdyl interacts with IRF4, which has been shown to promote M2 polarization.[34,35] As an important transcription factor involved in macrophage polarization, the inflammatory response, and SMC proliferation, IRF4 plays important roles in cardiovascular diseases, such as cardiomyopathy, myocardial infarction, and neointima formation.[40,45,46] Our results further revealed that circCdyl induces M1 polarization by preventing IRF4 from entering the nucleus through flow cytometry analysis and rescue experiments. Subsequently, we investigated another mechanism by which circCdyl regulates AAA formation. According to the bioinformatics analysis results, we predicted that circCdyl may regulate macrophage polarization by endogenously interacting with let-7c, which is expressed at low levels in AAA tissues and promotes M2 polarization by inhibiting C/EBP-δ expression.[32,33] In concert with our prediction, we successfully examined the interactions between let-7c and C/EBP-δ, circCdyl and let-7c, and circCdyl and C/EBP-δ in macrophages by luciferase reporter gene assays. In addition, C/EBP-δ expression was markedly inhibited by functional let-7c mimics or when circCdyl associated with let-7c. This inhibition was reversed when oe-circCdyl was present or when there was a crucial mutation in the circCdyl-let-7c or let-7c-C/EBP-δ base-pairing region. Therefore, we concluded that circCdyl acts as an endogenous let-7c sponge to regulate C/EBP-δ expression in macrophages. To investigate the association between the two mechanisms, we postulated two possible mechanisms based on the features of these two pathways: (1) IRF4 may regulate the circCdyl/let-7c/C/EBP-δ pathway by modulating circCdyl expression, thereby creating a feedback loop; and (2) IRF4 may affect C/EBP-δ expression by regulating let-7c. Subsequently, we designed additional experiments and observed that IRF4 had no role in regulating the expression of circCdyl, let-7c, and C/EBP-δ, indicating that these two pathways may have independent roles in promoting M1 polarization. Our mechanistic studies further demonstrated that circCdyl is a crucial regulator of AAA formation by controlling macrophage polarization.

We note certain limitations in this study. First, we used AAV infection to overexpress or knock down circCdyl in two AAA models. Although our results from AAV-infected mice consistently confirmed the effects of circCdyl on macrophage polarization and AAA development, the use of conventional genetic models to demonstrate our findings would be stricter. Second, the elucidation of upstream signaling pathways and a more specific mechanism of the regulation of circCdyl expression in AAA formation may require further investigation. Third, under the current circumstance that most patients are willing to choose interventional surgery rather than open surgery, we find it difficult to collect enough clinical samples for experimental use, which limited the clinical translation in the future.

In summary, upregulation of circRNA Cdyl stimulated the inflammatory response and promoted M1 polarization by inhibiting the entry of IRF4 into the nucleus and sponging let-7c to increase C/EBP-δ expression, significantly inducing AAA formation. Thus, the newly discovered circCdyl is likely to be a potential therapeutic target to prevent AAA formation.

MATERIALS AND METHODS

Data availability

The data, analytical methods, and study materials that support the findings of this study are available from the corresponding author on reasonable request.

Animal experiments

We obtained C57BL/6J mice and ApoE$^{-/-}$ mice from Southern Medical University. The mice were housed under pathogen-free conditions with a 12-h dark/12-h light cycle and fed a normal chow diet and water. All of the protocols for animal experiments were approved by the Animal Care and Use Committee of the Institute of Basic Medical Sciences, Chinese Academy of Medical Sciences, and Southern Medical University and are in accordance with the NIH Animal Research Advisory Committee Guidelines.

Ang II-infused AAA model

Male C57BL/6J mice and ApoE$^{-/-}$ mice aged 9–12 weeks were used in the experiment and randomly allocated into groups. The mice were anesthetized by injecting a combination of ketamine (100 mg/kg) and xylazine (5 mg/kg). Ang II (1.44 mg/kg/day, A9525, Sigma, USA) was

transfected with mimic-NC, let-7c mimic, inhibitor-NC, or let-7c inhibitor and then stimulated with LPS+IFN-γ (24 h). **p < 0.01; n = 5 per group. (F and G) C/EBP-δ protein levels in RAW264.7 cells transfected with oe-circCdyl or oe-vector and then stimulated with LPS+IFN-γ (24 h). **p < 0.01; n = 5 per group. (H and I) C/EBP-δ protein levels in RAW264.7 cells transfected with oe-vector + mimic-NC, oe-circCdyl + mimic-NC, oe-vector + let-7c mimic, or oe-circCdyl+let-7c mimic and then stimulated with LPS + IFN-γ (24 h). **p < 0.01; n = 5 per group. (J and K) C/EBP-δ protein levels in RAW264.7 cells transfected with si-scramble + inhibitor-NC, si-circCdyl + inhibitor-NC, si-scramble+let-7c inhibitor, or si-circCdyl+let-7c inhibitor and then stimulated with LPS+IFN-γ (24 h). **p < 0.01; n = 5 per group.

administered to mice using mini osmotic pumps (model 2004, Alzet, USA). Saline was used in the normal control group. The pumps were placed into the subcutaneous space of the dorsum of the neck. All mice were treated with Ang II or saline for 28 days.

$CaCl_2$-induced AAA model

Each mouse was fully anesthetized before the abdominal aorta was surgically exposed. $CaCl_2$-treated cotton gauze was then placed directly on the abdominal aorta at approximately the center of the section between the renal artery and the iliac bifurcation. Saline was used in a sham operation in the control mice. The gauze was removed after 15 min, and the incision was closed. The mice were euthanized at 3 weeks after $CaCl_2$ treatment, and the aortas were harvested for further analysis.

AAV infection in mice

Murine circCdyl-overexpression AAV2, circCdyl-knockdown AAV2, and the corresponding control AAV2 were all synthesized by GeneChem (Shanghai, China). For the *in vivo* studies, 1×10^{11} viral genome particles of AAV were delivered to the abdominal aorta through injection in the tail vein. The injected mice were subjected to AAA modeling after 30 days.

Systolic blood pressure measurement

Systolic blood pressure was measured using a tail-cuff instrument (BP-2010 blood pressure meter, Softron, Japan) every 7 days. In brief, the mice were fitted with a pneumatic pulse sensor on the tail and placed in a container. Systolic blood pressure was measured 1 day before Ang II treatment to determine the baseline value.

Aneurysm quantification

After 4 weeks of Ang II infusion, mice underwent whole-body perfusion-fixation via the left ventricle with 10% formaldehyde at physiological pressure. Then, the aortas were isolated and imaged for gross morphological assessments. The maximal aortic diameter was measured at the most dilated portion of the suprarenal aorta for the Ang II-induced model and the subrenal aorta for the $CaCl_2$-induced model using the digital images with Image-Pro Plus (Media Cybernetics). Measurements were performed at least three times by two coworkers blinded to the group information before analysis. Necropsies were performed if the mice died during the experiment. Aortic rupture was defined when there were blood clots in the thoracic cavity (thoracic aortic rupture) or in the retroperitoneal cavity (abdominal aortic rupture). Animals that died of aortic rupture were only used for calculating the mortality and were excluded from the analysis of maximal aortic diameter.

Flow cytometry

To determine the M1/M2 proportion in AAA lesions, aortas were cut into small pieces and then digested with 1× aorta dissociation enzyme stock solution (ADES) (125 U/mL collagenase type XI, 60 U/mL hyaluronidase type 1-s, 60 U/mL DNase I, and 450 U/mL collagenase type I in 2.5 mL of PBS; all enzymes are from Sigma-Aldrich) at 37°C for 1 h. The single-cell suspensions were prepared by shearing the aortas apart and passing them through a 70-μm cell strainer. The cells were collected by centrifugation and resuspended for further detection.

For flow cytometry analysis, cells were incubated with the following fluorochrome-labeled antibodies specific for surface markers: anti-F4/80-phycoerythrin (PE) (1:50, 123109, BioLegend) and anti-CD86-fluorescein isothiocyanate (FITC) (1:50, 105005, BioLegend). For intracellular staining, cells were fixed and permeabilized with fixation and permeabilization solution (BD Biosciences) for 20 min and then stained with an anti-CD206-allophycocyanin (APC) antibody (1:50, 141707, BioLegend). Then, cells were subjected to flow cytometry analysis, and the results were analyzed with FlowJo.

IHC staining

Abdominal aorta samples were used for histological analysis after macroscopic analysis. In brief, aortic samples were fixed in 10% formaldehyde and embedded in paraffin. Serial sections (5 μm each) at 500-mm intervals were prepared. Then, the aortic sections were deparaffinized, and endogenous peroxidase activity was blocked with 3% hydrogen peroxide, followed by incubation with 10% bovine serum to block nonspecific binding sites. The images were quantified with Image-Pro Plus software (Media Cybernetics, USA) by a researcher who was blinded to the group information. The primary antibodies used are available in Table S2.

ISH

ISH was performed using a Panomics QuantiGene ViewRNA for ISH tissue assay system (Affymetrix, Santa Clara, CA) to determine the expression and distribution of circCdyl in mouse aortic tissues. In brief, the aortic tissue sections were digested with proteinase K and then hybridized at 37°C overnight with a custom-designed circCdyl probe for mice. Then, the sections were incubated overnight with an anti-digoxin-alkaline phosphatase (AP) Fab fragment. The cytoplasm was stained with nitroblue tetrazolium (NBT)/5-bromo-4-chloro-3-indolyl phosphate (BCIP) in the dark, and circCdyl ISH signals were identified as blue-purple speckles.

EVG staining

EVG staining was performed as previously described. Serial sections of 5 μm were used for EVG staining. The grades for elastin degradation were evaluated following the previously described criteria: a score of 1 indicates no degradation of elastin, a score of 2 indicates mild degradation of elastin, a score of 3 indicates severe degradation of elastin, and a score of 4 indicates rupture of aorta.

Reverse transcriptase and qPCR

Total RNA was extracted with TRIzol (Invitrogen). One microgram of total RNA was used to synthesize cDNA using PrimeScript RT master mix (TaKaRa Biotechnology, Dalian, China). qPCR was performed with a SYBR Premix Ex Taq kit (TaKaRa Biotechnology, Dalian, China) using a LightCycler 480 II system (Roche Diagnostics, Basel, Switzerland). Glyceraldehyde-3-phosphate dehydrogenase (GAPDH) mRNA was used as an internal control to normalize

gene expression using the $2^{-\Delta\Delta Ct}$ method. Primer sequences are listed in Table S3.

Cytokine measurements

Mouse blood was collected from the abdominal aortas into tubes containing citrate-phosphate-dextrose anticoagulant and centrifuged to collect the plasma. Cytokine (TNF-α, MCP1, and IL-6) levels in plasma were determined by an enzyme-linked immunosorbent assay (ELISA) according to the manufacturer's protocol for each ELISA kit (Cusabio, Wuhan, Hubei, China). Optical density values were measured at a wavelength of 450 nm in an ELISA plate reader (Spectra Max M5, Molecular Devices, CA, United States).

Protein extraction and western blotting

Radioimmunoprecipitation assay (RIPA) buffer (25 mM Tris-HCl [pH 7.6], 150 mM NaCl, 1% Nonidet P40 [NP-40], 1% sodium deoxycholate, and 0.1% SDS) was used to extract protein. Briefly, the aorta tissues were snap-frozen in liquid nitrogen, pulverized by a homogenizer in RIPA buffer, sonicated, and centrifuged at 4°C. The supernatants were then collected. After protein concentrations were determined using a bicinchoninic acid (BCA) kit (23225, Thermo Fisher Scientific, USA), the samples were run on SDS-PAGE gels and then transferred onto polyvinylidene fluoride (PVDF) membranes. The membranes were blocked with 5% BSA in TBST at 37°C for 1 h and subsequently incubated with primary antibody at 4°C overnight. Then, the membranes were washed with Tris-buffered saline with Tween 20 (TBST), incubated with a horseradish peroxidase-conjugated secondary antibody, and detected with an enhanced chemiluminescence reagent (Advance, no. RPN2235; GE Healthcare Life Sciences). Western blots were replicated at least five times and quantified with ImageJ (National Institutes of Health, Bethesda, MD, USA). The intensity values were normalized to those of β-actin for total proteins and lamin B1 for nuclear proteins. Antibodies used for western blotting are available in Table S4.

Cell culture and treatment

The mouse macrophage cell line (RAW264.7 cells), the mouse aortic smooth muscle cell (AoSMC) line, the mouse endothelial cell (EC) line, and human THP-1 cell line were all purchased from Geneseed Biotech (Guangzhou, China). Cells were maintained in complete Dulbecco's modified Eagle's medium (DMEM, Gibco-BRL, USA) supplemented with 10% fetal bovine serum (FBS, Gibco-BRL), penicillin (100 U/mL), and streptomycin (100 mg/mL) in humidified air with 5% CO_2 at 37°C.

For the isolation of primary peritoneal macrophages, mice were intraperitoneally administered 1 mL of 4% thioglycolate. Three days later, cells were collected from peritoneal lavage and seeded into culture dishes with RPMI 1640 medium (Gibco-BRL, USA) containing 10% FBS and 1% penicillin/streptomycin and cultured in a cell incubator for 1 h. Then, the cells were washed with PBS, and nonadherent cells were discarded. The remaining adherent cells were macrophages.

For siRNA or overexpression plasmid transfection, the cells were seeded into six-well plates and cultured to a concentration of 10^6 cells/mL. The cells were then serum starved and transfected with a siRNA against circCdyl (circBase: hsa_circ_0008285/mmu_circ_0000451, http://www.circbase.org/) (si-circCdyl) or a circCdyl overexpression plasmid (oe-circCdyl) using Lipofectamine 2000 (Invitrogen, Thermo Fisher Scientific). After 6 h of incubation, the medium was replaced with DMEM supplemented with 10% FBS and 1% penicillin/streptomycin and the cells were cultured for 24 h.

RNA pulldown

The probes for circCdyl and its antisense RNA for RNA pull-down were designed and synthesized by Gzscbio (Guangzhou, China). Mouse RAW264.7 cells were washed in PBS, lysed in co-immunoprecipitation buffer, and then incubated with biotinylated DNA oligonucleotide probes against a circCdyl back-spliced sequence at room temperature for 4 h before being incubated with streptavidin-coated magnetic beads (Invitrogen, SA10004). Nonspecific binding of RNA and protein complexes was prevented using RNase-free BSA and yeast tRNA (Sigma, Shanghai, China). RNA complexes bound to beads were extracted with TRIzol for qRT-PCR analysis, and proteins were collected by SDS-PAGE and silver stained, with the specific bands excised and analyzed by mass spectrometry.

RIP

RIP experiments were performed using a Magna RIP RNA-binding protein immunoprecipitation kit (Millipore, Stafford, VA, USA) in accordance with the manufacturer's instructions. Anti-IRF4 antibodies were used to co-immunoprecipitate RNA, and circCdyl expression was measured by qRT-PCR.

Luciferase reporter assays

circCdyl-sv-wt and circCdyl-sv-mut were cloned into the luciferase vector psiCHECK-2 (Gzscbio, Guangzhou, China). For luciferase reporter assays, the let-7c mimic was cotransfected into RAW264.7 cells with the luciferase constructs described above using Lipofectamine 2000 (Invitrogen, Thermo Fisher Scientific). Luciferase activity was measured by the Dual-Luciferase reporter assay system (Promega, Madison, WI, USA).

Human tissue collection

All protocols using human aortic samples were approved by the Research Ethics Committees of Nanfang Hospital (ethical approval no. NFEC-2019-086). All procedures complied with the principles of the Declaration of Helsinki. Human tissue samples were collected from the abdominal aorta of patients undergoing open surgical repair. Aortic dissection or other inflammatory aortic disease had been excluded from these patients. Adjacent nonaneurysmal aortic segments were trimmed from the same patients and used as controls. The samples were flash-frozen in liquid nitrogen and stored at −80°C until RNA extraction was performed. Each subject signed written informed consent for collection of aortic samples for research purposes. Patient sex, age, smoking status, aortic diameter, and

related diseases were recorded (patient information is available in Table S1).

Ultrasonic imaging

Ultrasonic B-mode images of the aortas were obtained from mice anesthetized with 2% isoflurane using a Vevo 2100 imaging system (Visual Sonics, ON, Canada) equipped with a 40-MHz probe. Ultrasonic imaging was performed 1 day before model establishment as baseline and then measured on the 14th and 28th days. The aortic lumen diameters were measured (corresponding to cardiac systole) three times on the long axis of the suprarenal abdominal aorta by a blinded investigator. Data for the diastolic abdominal aortic lumen diameter are shown for individual animals.

Statistical analysis

Quantitative results are expressed as the means ± SD. The elastin degradation scores are presented as medians and quartiles. The normality and homogeneity of variance in the data were assessed for multiple comparisons, and a Kruskal-Wallis test plus a post hoc analysis (Dunn multiple comparison test) was used for variables that did not pass a normality or equal variance test. Fisher's exact test was applied to the comparisons of AAA incidence, and the log-rank (Mantel-Cox) test was used for survival analysis. Graphs were created using Prism 6.0 (GraphPad), and statistical analysis was performed with GraphPad Prism. A $p < 0.05$ was considered to be statistically significant.

SUPPLEMENTAL INFORMATION

Supplemental information can be found online at https://doi.org/10.1016/j.ymthe.2021.09.017.

ACKNOWLEDGMENTS

This work was supported by grants awarded to J.B. from the National Natural Science Foundation of China (nos. 82070315 and 81771857) and the Guangzhou Regenerative Medicine and Health Laboratory of Guangdong (2018GZR110105009). This work was also supported by an award from the National Natural Science Foundation of China to L.Z. (no. 82000431).

AUTHOR CONTRIBUTIONS

H.S. and Y.Y. wrote the manuscript, performed the experiments, and analyzed the data; Y.S., G.W., H.Z., Y.C., and D.C. performed the experiments and analyzed the data; C.L., Y.M., Z.L., and X.S. analyzed the data and wrote the manuscript; W.L., Y.L., and L.Z. designed the research; and J.B. designed the research and wrote the manuscript. All authors read and approved the final version of the manuscript.

DECLARATION OF INTERESTS

The authors declare no competing interests.

REFERENCES

1. Golledge, J., Muller, J., Daugherty, A., and Norman, P. (2006). Abdominal aortic aneurysm: Pathogenesis and implications for management. Arterioscler. Thromb. Vasc. Biol. *26*, 2605–2613.
2. Nordon, I.M., Hinchliffe, R.J., Loftus, I.M., and Thompson, M.M. (2011). Pathophysiology and epidemiology of abdominal aortic aneurysms. Nat. Rev. Cardiol. *8*, 92–102.
3. Rizas, K.D., Ippagunta, N., and Tilson, M.D., 3rd (2009). Immune cells and molecular mediators in the pathogenesis of the abdominal aortic aneurysm. Cardiol. Rev. *17*, 201–210.
4. Raffort, J., Lareyre, F., Clément, M., Hassen-Khodja, R., Chinetti, G., and Mallat, Z. (2017). Monocytes and macrophages in abdominal aortic aneurysm. Nat. Rev. Cardiol. *14*, 457–471.
5. Kim, W., Lee, E.J., Bae, I.H., Myoung, K., Kim, S.T., Park, P.J., Lee, K.H., Pham, A.V.Q., Ko, J., Oh, S.H., and Cho, E.G. (2020). *Lactobacillus plantarum*-derived extracellular vesicles induce anti-inflammatory M2 macrophage polarization *in vitro*. J. Extracell. Vesicles *9*, 1793514.
6. Murray, P.J., Allen, J.E., Biswas, S.K., Fisher, E.A., Gilroy, D.W., Goerdt, S., Gordon, S., Hamilton, J.A., Ivashkiv, L.B., Lawrence, T., et al. (2014). Macrophage activation and polarization: Nomenclature and experimental guidelines. Immunity *41*, 14–20.
7. Chinetti-Gbaguidi, G., Colin, S., and Staels, B. (2015). Macrophage subsets in atherosclerosis. Nat. Rev. Cardiol. *12*, 10–17.
8. Zhou, Z.B., Huang, G.X., Fu, Q., Han, B., Lu, J.J., Chen, A.M., and Zhu, L. (2019). circRNA.33186 contributes to the pathogenesis of osteoarthritis by sponging miR-127-5p. Mol. Ther. *27*, 531–541.
9. Cao, Q., Wang, C., Zheng, D., Wang, Y., Lee, V.W., Wang, Y.M., Zheng, G., Tan, T.K., Yu, D., Alexander, S.I., et al. (2011). IL-25 induces M2 macrophages and reduces renal injury in proteinuric kidney disease. J. Am. Soc. Nephrol. *22*, 1229–1239.
10. Chen, T., Cao, Q., Wang, Y., and Harris, D.C.H. (2019). M2 macrophages in kidney disease: Biology, therapies, and perspectives. Kidney Int. *95*, 760–773.
11. Zhou, X., Li, W., Wang, S., Zhang, P., Wang, Q., Xiao, J., Zhang, C., Zheng, X., Xu, X., Xue, S., et al. (2019). YAP aggravates inflammatory bowel disease by regulating M1/M2 macrophage polarization and gut microbial homeostasis. Cell Rep. *27*, 1176–1189.e5.
12. Soliman, E., Elhassanny, A.E.M., Malur, A., McPeek, M., Bell, A., Leffler, N., Van Dross, R., Jones, J.L., Malur, A.G., and Thomassen, M.J. (2020). Impaired mitochondrial function of alveolar macrophages in carbon nanotube-induced chronic pulmonary granulomatous disease. Toxicology *445*, 152598.
13. Sakaue, T., Suzuki, J., Hamaguchi, M., Suehiro, C., Tanino, A., Nagao, T., Uetani, T., Aono, J., Nakaoka, H., Kurata, M., et al. (2017). Perivascular adipose tissue angiotensin II type 1 receptor promotes vascular inflammation and aneurysm formation. Hypertension *70*, 780–789.
14. Dale, M.A., Ruhlman, M.K., and Baxter, B.T. (2015). Inflammatory cell phenotypes in AAAs: Their role and potential as targets for therapy. Arterioscler. Thromb. Vasc. Biol. *35*, 1746–1755.
15. Shi, X., Ma, W., Li, Y., Wang, H., Pan, S., Tian, Y., Xu, C., and Li, L. (2020). miR-144-5p limits experimental abdominal aortic aneurysm formation by mitigating M1 macrophage-associated inflammation: Suppression of TLR2 and OLR1. J. Mol. Cell. Cardiol. *143*, 1–14.
16. Zhang, Z., Xu, J., Liu, Y., Wang, T., Pei, J., Cheng, L., Hao, D., Zhao, X., Chen, H.Z., and Liu, D.P. (2018). Mouse macrophage specific knockout of *SIRT1* influences macrophage polarization and promotes angiotensin II-induced abdominal aortic aneurysm formation. J. Genet. Genomics *45*, 25–32.
17. Batra, R., Suh, M.K., Carson, J.S., Dale, M.A., Meisinger, T.M., Fitzgerald, M., Opperman, P.J., Luo, J., Pipinos, I.I., Xiong, W., and Baxter, B.T. (2018). IL-1β (interleukin-1β) and TNF-α (tumor necrosis factor-α) impact abdominal aortic aneurysm formation by differential effects on macrophage polarization. Arterioscler. Thromb. Vasc. Biol. *38*, 457–463.
18. Zhao, J., Li, X., Hu, J., Chen, F., Qiao, S., Sun, X., Gao, L., Xie, J., and Xu, B. (2019). Mesenchymal stromal cell-derived exosomes attenuate myocardial ischaemia-reperfusion injury through miR-182-regulated macrophage polarization. Cardiovasc. Res. *115*, 1205–1216.
19. Wei, Y., Corbalán-Campos, J., Gurung, R., Natarelli, L., Zhu, M., Exner, N., Erhard, F., Greulich, F., Geißler, C., Uhlenhaut, N.H., et al. (2018). Dicer in macrophages prevents atherosclerosis by promoting mitochondrial oxidative metabolism. Circulation *138*, 2007–2020.

20. Xue, Y.L., Zhang, S.X., Zheng, C.F., Li, Y.F., Zhang, L.H., Su, Q.Y., Hao, Y.F., Wang, S., and Li, X.W. (2020). Long non-coding RNA MEG3 inhibits M2 macrophage polarization by activating TRAF6 via microRNA-223 down-regulation in viral myocarditis. J. Cell. Mol. Med. *24*, 12341–12354.

21. Arnaiz, E., Sole, C., Manterola, L., Iparraguirre, L., Otaegui, D., and Lawrie, C.H. (2019). circRNAs and cancer: Biomarkers and master regulators. Semin. Cancer Biol. *58*, 90–99.

22. Qu, S., Yang, X., Li, X., Wang, J., Gao, Y., Shang, R., Sun, W., Dou, K., and Li, H. (2015). Circular RNA: A new star of noncoding RNAs. Cancer Lett. *365*, 141–148.

23. Hansen, T.B., Jensen, T.I., Clausen, B.H., Bramsen, J.B., Finsen, B., Damgaard, C.K., and Kjems, J. (2013). Natural RNA circles function as efficient microRNA sponges. Nature *495*, 384–388.

24. Du, W.W., Yang, W., Liu, E., Yang, Z., Dhaliwal, P., and Yang, B.B. (2016). Foxo3 circular RNA retards cell cycle progression via forming ternary complexes with p21 and CDK2. Nucleic Acids Res. *44*, 2846–2858.

25. Kong, P., Yu, Y., Wang, L., Dou, Y.Q., Zhang, X.H., Cui, Y., Wang, H.Y., Yong, Y.T., Liu, Y.B., Hu, H.J., et al. (2019). circ-Sirt1 controls NF-κB activation via sequence-specific interaction and enhancement of SIRT1 expression by binding to miR-132/212 in vascular smooth muscle cells. Nucleic Acids Res. *47*, 3580–3593.

26. Li, X., Yang, L., and Chen, L.L. (2018). The biogenesis, functions, and challenges of circular RNAs. Mol. Cell *71*, 428–442.

27. Li, M., Hua, Q., Shao, Y., Zeng, H., Liu, Y., Diao, Q., Zhang, H., Qiu, M., Zhu, J., Li, X., et al. (2020). Circular RNA circBbs9 promotes $PM_{2.5}$-induced lung inflammation in mice via NLRP3 inflammasome activation. Environ. Int. *143*, 105976.

28. Lu, X., Liu, Y., Xuan, W., Ye, J., Yao, H., Huang, C., and Li, J. (2019). circ_1639 induces cells inflammation responses by sponging miR-122 and regulating TNFRSF13C expression in alcoholic liver disease. Toxicol. Lett. *314*, 89–97.

29. Zhang, Z., Zhang, T., Feng, R., Huang, H., Xia, T., and Sun, C. (2019). circARF3 alleviates mitophagy-mediated inflammation by targeting miR-103/TRAF3 in mouse adipose tissue. Mol. Ther. Nucleic Acids *14*, 192–203.

30. Holdt, L.M., Stahringer, A., Sass, K., Pichler, G., Kulak, N.A., Wilfert, W., Kohlmaier, A., Herbst, A., Northoff, B.H., Nicolaou, A., et al. (2016). Circular non-coding RNA ANRIL modulates ribosomal RNA maturation and atherosclerosis in humans. Nat. Commun. *7*, 12429.

31. Zhang, Y., Zhang, Y., Li, X., Zhang, M., and Lv, K. (2017). Microarray analysis of circular RNA expression patterns in polarized macrophages. Int. J. Mol. Med. *39*, 373–379.

32. Kin, K., Miyagawa, S., Fukushima, S., Shirakawa, Y., Torikai, K., Shimamura, K., Daimon, T., Kawahara, Y., Kuratani, T., and Sawa, Y. (2012). Tissue- and plasma-specific microRNA signatures for atherosclerotic abdominal aortic aneurysm. J. Am. Heart Assoc. *1*, e000745.

33. Banerjee, S., Xie, N., Cui, H., Tan, Z., Yang, S., Icyuz, M., Abraham, E., and Liu, G. (2013). MicroRNA let-7c regulates macrophage polarization. J. Immunol. *190*, 6542–6549.

34. Eguchi, J., Kong, X., Tenta, M., Wang, X., Kang, S., and Rosen, E.D. (2013). Interferon regulatory factor 4 regulates obesity-induced inflammation through regulation of adipose tissue macrophage polarization. Diabetes *62*, 3394–3403.

35. Wang, F., Sun, F., Luo, J., Yue, T., Chen, L., Zhou, H., Zhang, J., Yang, C., Luo, X., Zhou, Q., et al. (2019). Loss of ubiquitin-conjugating enzyme E2 (Ubc9) in macrophages exacerbates multiple low-dose streptozotocin-induced diabetes by attenuating M2 macrophage polarization. Cell Death Dis. *10*, 892.

36. Song, H., Xu, T., Feng, X., Lai, Y., Yang, Y., Zheng, H., He, X., Wei, G., Liao, W., Liao, Y., et al. (2020). Itaconate prevents abdominal aortic aneurysm formation through inhibiting inflammation via activation of Nrf2. EBioMedicine *57*, 102832.

37. Fu, Y., Gao, C., Liang, Y., Wang, M., Huang, Y., Ma, W., Li, T., Jia, Y., Yu, F., Zhu, W., et al. (2016). Shift of macrophage phenotype due to cartilage oligomeric matrix protein deficiency drives atherosclerotic calcification. Circ. Res. *119*, 261–276.

38. Singh, K., Bønaa, K.H., Jacobsen, B.K., Bjørk, L., and Solberg, S. (2001). Prevalence of and risk factors for abdominal aortic aneurysms in a population-based study: The Tromsø Study. Am. J. Epidemiol. *154*, 236–244.

39. Forsdahl, S.H., Singh, K., Solberg, S., and Jacobsen, B.K. (2009). Risk factors for abdominal aortic aneurysms: A 7-year prospective study: the Tromsø Study, 1994–2001. Circulation *119*, 2202–2208.

40. Cheng, W.L., She, Z.G., Qin, J.J., Guo, J.H., Gong, F.H., Zhang, P., Fang, C., Tian, S., Zhu, X.Y., Gong, J., et al. (2017). Interferon regulatory factor 4 inhibits neointima formation by engaging Krüppel-like factor 4 signaling. Circulation *136*, 1412–1433.

41. Deng, G.G., Martin-McNulty, B., Sukovich, D.A., Freay, A., Halks-Miller, M., Thinnes, T., Loskutoff, D.J., Carmeliet, P., Dole, W.P., and Wang, Y.X. (2003). Urokinase-type plasminogen activator plays a critical role in angiotensin II-induced abdominal aortic aneurysm. Circ. Res. *92*, 510–517.

42. King, V.L., Trivedi, D.B., Gitlin, J.M., and Loftin, C.D. (2006). Selective cyclooxygenase-2 inhibition with celecoxib decreases angiotensin II-induced abdominal aortic aneurysm formation in mice. Arterioscler. Thromb. Vasc. Biol. *26*, 1137–1143.

43. Shu, Y.N., Dong, L.H., Li, H., Pei, Q.Q., Miao, S.B., Zhang, F., Zhang, D.D., Chen, R., Yin, Y.J., Lin, Y.L., et al. (2017). CKII-SIRT1-SM22α loop evokes a self-limited inflammatory response in vascular smooth muscle cells. Cardiovasc. Res. *113*, 1198–1207.

44. Chen, H.Z., Wang, F., Gao, P., Pei, J.F., Liu, Y., Xu, T.T., Tang, X., Fu, W.Y., Lu, J., Yan, Y.F., et al. (2016). Age-associated sirtuin 1 reduction in vascular smooth muscle links vascular senescence and inflammation to abdominal aortic aneurysm. Circ. Res. *119*, 1076–1088.

45. Liu, X., Chen, J., Zhang, B., Liu, G., Zhao, H., and Hu, Q. (2019). KDM3A inhibition modulates macrophage polarization to aggravate post-MI injuries and accelerates adverse ventricular remodeling via an IRF4 signaling pathway. Cell. Signal. *64*, 109415.

46. Jiang, D.S., Bian, Z.Y., Zhang, Y., Zhang, S.M., Liu, Y., Zhang, R., Chen, Y., Yang, Q., Zhang, X.D., Fan, G.C., and Li, H. (2013). Role of interferon regulatory factor 4 in the regulation of pathological cardiac hypertrophy. Hypertension *61*, 1193–1202.